

FLOW AND HEAT-TRANSFER CHARACTERISTICS IN SMALL-DIAMETER TUBE BUNDLES WITH A STAGGERED LAYOUT: AN EXPERIMENTAL STUDY

Han Qi,^{1,2,3} Guoqiang Xu,^{1,2,3} Weitong Liu,^{1,2,3} Lina Zhang,^{1,2,4} & Yanchen Fu^{1,2,4,5,*}

¹*Research Institute of Aero-Engine, Beihang University, Beijing 100191, China*

²*National Key Laboratory of Science and Technology on Aero-Engine Aero-Thermodynamics, Beihang University, Beijing 100191, China*

³*School of Energy and Power Engineering, Beihang University, Beijing 100191, China*

⁴*Frontiers Science Center for Super-Cycle Aeroengine's Aerothermodynamics, Beihang University, Beijing 100191, China*

⁵*Collaborative Innovation Center for Advanced Aero-Engine, Beihang University, Beijing 100191, China*

*Address all correspondence to: Yanchen Fu, Research Institute of Aero-Engine, Beihang University, Beijing 100191, China; Tel.: +86 13811460810; Fax: +010-61716914; E-mail: yanchenfu@buaa.edu.cn

Original Manuscript Submitted: 9/7/2023; Final Draft Received: 1/4/2024

While past research has primarily focused on heat transfer in larger diameter tubes, the capabilities of small-diameter tubes have often been estimated using correction factors. However, with the evolution of compact heat exchangers, conducting dedicated studies on small-diameter tube bundles has become increasingly crucial to achieve more precise conclusions. An experimental research on flow and heat-transfer characteristics of staggered tube bundles with different tube diameters (2, 3, and 5 mm) is conducted. In the experiment, the number of rows (4–12), the mass rate of the air (0.06–0.18 kg/s), and the transverse tube pitch ($S_t/d = 2, S_t/d = 3$) are variables to study the characteristics of the airside flow resistance and heat transfer. The three main conclusions of the experimental results are as follows: (1) Under the same conditions, the smaller tube diameter leads to the larger airside convective heat-transfer coefficient. Besides, the deviation between the Nusselt number of the experiment and the empirical correlation of Žukauskas is in the range between -14 and -10%; (2) The effect of transverse distance on heat transfer is not obvious, but the convective heat-transfer coefficient increases significantly with the increase of row number; (3) The external pressure drop of the tube exhibits an exponential increase with the air-flow rate. Particularly in the experimental samples with smaller diameters, the outflow resistance of the tube is noticeably higher compared to other tubes. Finally, new empirical correlations of the airside convection heat transfer for the small-diameter staggered tube bundles are fitted according to the experimental data, and it is hoped to provide a reference for the more accurate design of tube-bundle heat exchangers.

KEY WORDS: *tube bundle, heat transfer, pressure drop, small diameter, staggered row*

NOMENCLATURE

A	flow area (m^2)	δ	constant of correlations
A_t	test section area (m^2)	γ	constant of correlations
c_p	isobaric specific heat capacity [$\text{kJ}/(\text{kg}\cdot\text{K})$]	λ	thermal conductivity [$\text{W}/(\text{m}\cdot\text{K})$]
d	tube diameter (m)	μ	dynamic viscosity ($\text{Pa}\cdot\text{s}$)
Eu	Euler number	ρ	density (kg/m^3)
f	Fanning friction factor	σ	uncertainty
h	convective heat-transfer coefficient [$\text{W}/(\text{m}^2\cdot\text{K})$]		
l	tube length (m)	Subscripts	
m	mass-flow rate (kg/s)	a	air
N_t	tube row numbers	ave	average
Nu	Nusselt number	cal	calculate
P	pressure (MPa)	cor	correction
Pr	Prandtl number	exp	experimental
Q	heat flux (W)	i	inside
Re	Reynolds number	in	inlet
S	heat-transfer area (m^2)	max	maximum
S_1	transverse distance (m)	min	minimum
S_2	longitudinal distance (m)	o	outside
T	temperature (K)	out	outlet
T_w	tube-wall temperature (K)	$tube$	tube
T_f	air temperature (K)	w	wall
V	velocity of flow (m/s)		
Greek			
α	constant of correlations		
β	constant of correlations		
Abbreviations			
CCA cooled cooling air			
HTC heat-transfer coefficient			
HX heat exchanger			
LMTD logarithmic mean temperature difference			

1. INTRODUCTION

The rapid advancement of hypersonic vehicles in recent years has led to increased demands for higher performance, posing new challenges to the thermal protection capabilities of their power systems. A sophisticated cooling technology called Cooled Cooling Air (CCA) has been proposed by Bruening (1999) for the thermal protection of turbine hot-end components of aero engines in last decades. More specifically, by installing a heat exchanger on engines allows the heat exchange between the onboard fuel and inlet air to improve its cooling efficiency (Fu et al., 2024). The tube-bundle heat exchangers utilized in aeronautical engines typically possess several distinct features, such as more compact, lower weight, robust reliability, and high thermal transfer efficiency. Consequently, the study of convective heat-transfer characteristics in tube rows, with varying diameters and arrangements, and their influence on the efficiency of tube-bundle heat exchangers has garnered significant attention.

In the realm of heat-transfer research, the study of forced convection across multiple-bank tube bundles has been a topic of both numerical and experimental investigation for many decades. This research primarily focuses on the advantages and disadvantages of different tube-

bundle arrangements, specifically the in-line configuration where tubes are arranged in a single row in parallel and the staggered configuration where tubes are offset in alternating rows. The investigation into how varying tube diameters influence heat transfer and pressure drop, subsequently affecting heat-exchanger performance, represents a crucial area of study. Most studies have focused on conventional tube-bundle diameters (≥ 10 mm), the applicability of which to miniature tube-bundle forked row structure heat exchangers remains to be discussed (Li et al., 2022; Wung and Chen, 1989; Khan et al., 2006). Of interest is the small-diameter tube row with a diameter of 5 mm, which is especially suitable for compact heat exchangers used within aircraft engines.

Žukauskas (1987) completed the initial experimental work on aligned and staggered bundles and established a complete empirical relationship for heat transfer. The empirical correlations have received widespread recognition and acceptance in the academic community. Qiwu and Yangke (2010) verified the Žukauskas empirical formula by numerical simulation, while the deviation is less than 5%. The configuration of tube bundles has been a topic of interest in research, with the findings indicating that staggered tube bundles offer better thermal-hydraulic performance compared to in-line arrangements, albeit with a slightly higher pressure drop (Zhang et al., 1997; Chen et al., 2000). Pan et al. (2004) and Da-Peng et al. (2003) have carried out series of numerical investigations to assess the flow-field characteristics of non-uniform incoming air across both aligned and staggered tube bundles. The results revealed that the disturbance of the staggered bundle on the incoming air was more pronounced than that of the aligned bundle under comparable conditions, and by varying the tube spacing can effectively mitigate the flow loss. In the study conducted by Saraireh et al. (2017), three-dimensional computational fluid-dynamics simulations were performed to investigate the impact of air velocity and heat flux on staggered and in-line tube arrangements. The results indicate that compact banks, whether in-line or staggered, exhibit higher heat transfer compared to widely spaced configurations. Recent research by scholars (Khan et al., 2021) has focused on the thermohydraulic behavior of staggered twisted oval tube (TWT) bundles in air-water cross flows, identifying a need for more comprehensive computational studies and design optimization. Due to the intricate nature of inter-tube flow, a majority of theoretical analyses and simulation studies have utilized simplified boundary conditions, resulting in their limited applicability to laminar flow conditions (Liu et al., 2023; Xie et al., 2020). Zhao et al. (2022) were also interested in the effects of tube spacing and tube-bundle arrangement on the fluid dynamics and heat-transfer properties of falling film in tube bundles and carried out numerical studies.

The investigation of heat transfer in tube bundles has practical applications in determining the thermodynamic characteristics of heat exchangers. Wilson and Bassiouny (2000) performed numerical investigations on the heat transfer and friction factor of cross-flow heat exchangers with in-line and staggered arrangements. Their results demonstrated that the Nusselt number for the staggered arrangement is somewhat higher than that of the in-line arrangement, particularly in the low range of S/d . Xu et al. (2016) investigated the effect of pipe diameter on the convective heat transfer of a cross-row tube-bundle heat exchanger through theoretical calculation. The study used a tube diameter of 20 mm in the model. Results showed that as the tube diameter decreases, the heat transfer increases, air outlet temperature decreases, and the heat-transfer enhancement is significant. In other words, smaller tube diameter leads to a greater enhancement in convective heat transfer. Zeenshan et al. (2020) numerically investigated the effect of tube shape variation on the thermal and flow characteristics of fin and tube heat exchangers. Their results indicate that the overall performance of the system increases as the tube aspect ratio decreases for all studied cases. Qing et al. (2007) investigated the impact of the trailing edge spoiler channel arrangement in turbine blades on heat transfer and flow characteristics using 3D numerical simulations. The results indicated that a staggered configuration along the flow direction was found to be the optimal arrangement method. The study by Wung and Chen (Wung and Chen, 1989; Chen and Wung, 1989) investigated the temperature field, heat-transfer characteristics, and pressure drop in aligned

and staggered tube bundles by solving the convective flow. Results showed that the heat-transfer rate outside the staggered tube bundle was higher than that in the aligned tube bundle, although the staggered tubes also displayed increased outflow resistance. Other studies (Deeb, 2022) have explored the enhanced thermal-hydraulic performance of heat exchangers using drop-shaped tubes, emphasizing their efficiency over traditional circular tubes in varied pitch ratio settings.

In addition to these numerical methods, the researchers also conducted experimental studies on the tube-bundle heat-transfer issue. Lai et al. (2019) investigated the cross-flow effects on fluid-elastic instability in steam generator tube bundles, revealing two critical states of stability and corresponding critical velocities through both experimental and numerical analyses. Fei et al. (2014) engaged in experimental investigations on the effect of the number of tube rows and bundle arrangement. Results demonstrated heat transfer increased with more tube rows, reaching a plateau at 10 rows. Additionally, the dimensionless Euler number of flow resistance was found to decrease with the increasing number of tube rows, and the staggered bundle had higher heat transfer but greater resistance than the anterograde bundle, as confirmed by numerical simulation. Grimison (1937) observed that the convective heat-transfer rate outside the tube was not immediately in a steady state; however, it increased with the increasing number of tube rows. Upon reaching a row number of 10, the convective heat-transfer rate achieved a relatively stable state. He formulated a widely utilized equation, $Nu = CRe^n$, which represented his findings. An experimental work (Wu et al., 2020) focused on the heat-transfer characteristics of staggered tube-bundle heat exchangers in oscillating flow, proposing a new Nusselt number correlation that accounts for wave parameters and depth, enhancing the design of seawater heat exchangers. However, the tube diameters investigated in the aforementioned studies were all greater than 10 mm. In the latest research of Yangjia et al. (2023) numerically investigates the flow and heat-transfer characteristics of small-scale staggered tube bundles in cross flow to assess the validity of classical heat-transfer correlations. It was concluded that tube diameter minimally affects the Nusselt number, while tube pitch ratio and Reynolds number significantly influence heat transfer. et al. Ishak et al. (2013) presented an experimental investigation on laminar forced convection air flow in a staggered flat tube bank in cross flow, and discovered a new correlation between the mean Nusselt number and Reynolds number.

Recent experimental (Li et al., 2017; Wen et al., 2017; Liu et al., 2018, 2022) findings reveal that the air-side heat transfer and pressure drop of heat exchangers with small-diameter tube bundles (less than 4 mm) exhibit some deviation (approximately -16%) from the reference empirical equation. Bacellar et al. (2014) identified a dearth of experimental research on heat transfer outside tubes with diameters below 5mm, which is highly valuable for compact tube heat exchangers. To bridge the gap, Bacellar et al. (2016) employed numerical simulations to investigate tube bundles ranging from 0.5–2 mm, which were validated by experimental data. The findings indicate good agreement between the simulation and experiment at high Reynolds numbers, but a deviation of up to 15% at low Reynolds numbers. In their experimental study, Chang et al. (2015) investigated the difference between the flow heat-transfer characteristics of a tube bundle and the corresponding empirical formula. The experimental conditions involved a tube diameter of 7.94 mm and a tube row number of 10, and the measured heat transfer was found to be 10–16% lower than the predicted values. The recurring observation highlights the limited utility of conventional equations for small tubular diameters.

In this study, the thermal characteristics of tubular rows with smaller diameters are explored to provide theoretical support for the design of compact heat exchangers. Specifically, the effects of the incoming air-flow Reynolds number, tube diameter, number of tube rows, and transverse distance S_t between tubes are investigated. The experimental method involves heating the tube bundle using constant current, achieving a higher temperature state, and then passing room-temperature air across the tube bundle. By measuring the temperature of the tube wall, the temperature difference between the inlet and outlet, and the pressure drop of the experimental section, new coefficients are proposed to establish a mathematical model with wider applicability.

2. EXPERIMENTAL SETUPS

2.1 Experimental Apparatus

The heating tube used in the experimental section is shown in Fig. 1. A core consisting of staggered bundles that are sequentially secured on the base forms the main part of the experimental section. A total of 12 rows are employed, with each row containing 6 small bundles, as depicted in Fig. 1. The diameter and transverse distance, S_1 , of these bundles are identified as variable parameters under investigation, and are tabulated below.

To ensure excellent heat transfer and insulation properties of the experimental apparatus, the structure of the tube bundle, depicted in Fig. 2, consists of a copper tube, a heat-conducting ceramic tube, and a heating wire, arranged from the outside to the inside. The copper tube, with excellent thermal conductivity, facilitates temperature measurement and recording. The specially designed ceramic tube, featuring a thermal conductivity of approximately $20 \text{ W}/(\text{m} \cdot \text{K})$, enables effective heat conduction and electrical insulation between the outermost copper tube and the innermost heating-wire layer, made of a nickel-chromium alloy that delivers exceptional heating performance and current-carrying capacity. During fabrication, we use 12 cm long and 0.2 mm diameter nickel-chromium alloy as the heating wire and pass it through a 10 cm long thermal conductive ceramic tube with an inner diameter of 0.3 mm. The gap between the two is filled with thermal grease. The ceramic tube, equipped with the heating wire, is then inserted into a

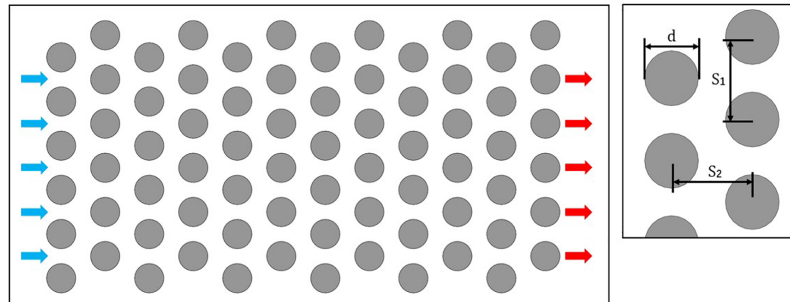


FIG. 1: Physical diagram and arrangement of the tube bundle

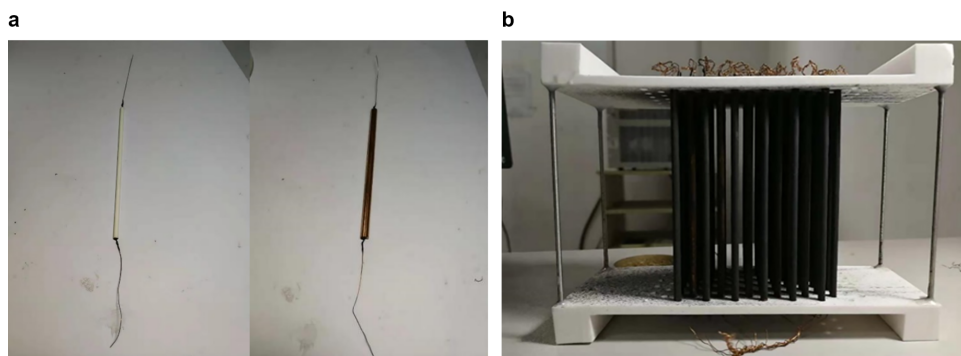


FIG. 2: Structure of the tube and test section: (a) tubes that can be used for experiments, and (b) core composed of multiple tube bundles

copper tube with the same outer diameter. Subsequently, both ports of the copper tube are fixed and sealed with high-temperature adhesive. Finally, the part of the heating wire that exceeds the length of the ceramic tube is wound and connected with the copper wire with a diameter of 0.3 mm, and the use of glue will ensure that they are connected tightly. After the tube bundle is installed on the base and connected to the external power supply, the experimental core is fully assembled. In the experiment, each heating wire in the device is connected in parallel with the power supply by a wire to ensure that the core is heated by an electric current.

2.2 Experimental Bench

Figure 3 depicts a schematic diagram of the experimental system, which comprised several key components, including the air system, heating system, measurement system, experimental core, and data acquisition system, as shown in the test platform. All the brands and models of the equipment are listed in Table 1. A mechanical valve is utilized to regulate the air flow at the outlet of the fan, ensuring a consistent and steady flow throughout the experiment. To promote adequate air-flow development through the test section, a long air runner is positioned in front of the test section. The heat source that has been heated by applying electric power to the core is a DC power source with a constant 30 V voltage, because it is connected in parallel with each heat-

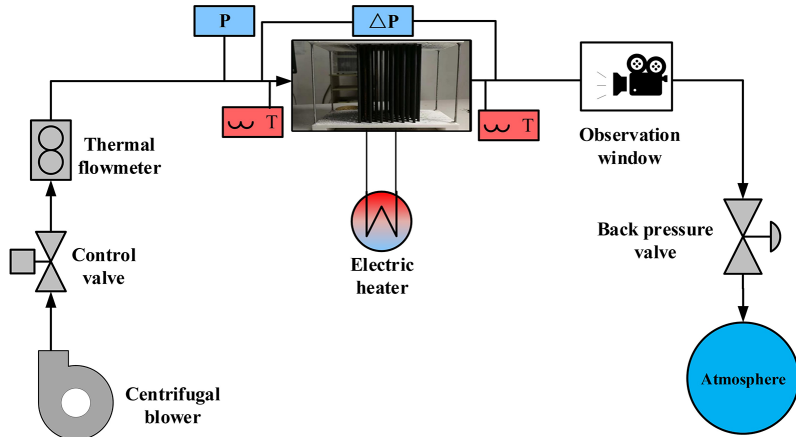


FIG. 3: Schematic of the experimental system

TABLE 1: Experimental equipment brand and model

Measuring instrument	Brand	Model
Flowmeter	Milon Instrument	MLRSL-100-C1C031
Thermocouple	Omega Engineering	TT-T-30-1000
Infrared thermal imager	FLIR-SYSTEMS-INC	FLIR-SC7700BB
Differential pressure gauge	Rosemount	3051CD4
Absolute pressure gauge	Rosemount	3051CA4
Precision multimeter	ESCORT	3146A
Acquisition card	Advantech	ADAM-4018/4520

ing wire, so its heating power is all the same. The measurement system consists of a flowmeter, pressure transmitter, and thermocouple. To minimize temperature-measurement errors, multiple T-type thermocouple is chosen to measure temperature, with its ends welded to the inlet and outlet of the test section, respectively. The temperature difference is calculated based on the potential difference of a single thermocouple, with an accuracy of 0.5% maintained. Twelve temperature measurement points were strategically positioned along the circumference of the inlet and outlet of the experimental section to ensure precise determination of the temperature field without impeding the flow. The model of the inlet and outlet components, along with the placement of the measurement points and the specific distribution of thermocouples, are illustrated in Fig. 4. To ensure accuracy, we employed the ice bath method for cold-junction compensation, immersing the thermocouples in a stable, near-freezing environment (0 degrees Celsius) to calibrate and compensate for variations in the cold-junction temperature. Additionally, an infrared thermal imager is employed to measure the wall temperature of the heating tube bundle in the experimental section. The imager is positioned in the observation window and continuously records the data throughout the experiment.

Before commencing the experiment, it is imperative to employ a multimeter to verify the normalcy of the resistance value of each heating tube. Subsequently, the appropriate tube bundle should be inserted into the heating base, followed by the application of black-body spray paint on the surface of the tube bundle. Once the bundle is installed in the designated test section, the wires should be connected to the DC power supply to complete the setup process.

In the initial experiment phase, all essential instruments are powered on, including the sequential activation of the infrared thermal imager following a 5 min preheating period. The air mass-flow rate is then adjusted to the required value, and the DC heating power supply is activated, with the voltage set to 30 V based on the precision multimeter reading. After completing these initial steps, all bolts on the experimental section are tightened, and the ice bottle is prepared for the formal experiment, with the thermocouple's reference end inserted into the alcohol test tube within the ice bottle. In the subsequent experimental phase, the air-inlet temperature of the experimental section is carefully monitored until stabilization, usually taking approximately 15 min. Once the air-inlet temperature stabilizes, potential values of thermocouples 1–12 are measured and recorded using the precision multimeter. These values are input into the data acquisition software on the desktop computer, and compliance with heat-balance requirements is assessed, ensuring deviations do not exceed 10%. The air mass-flow rate is adjusted, and the

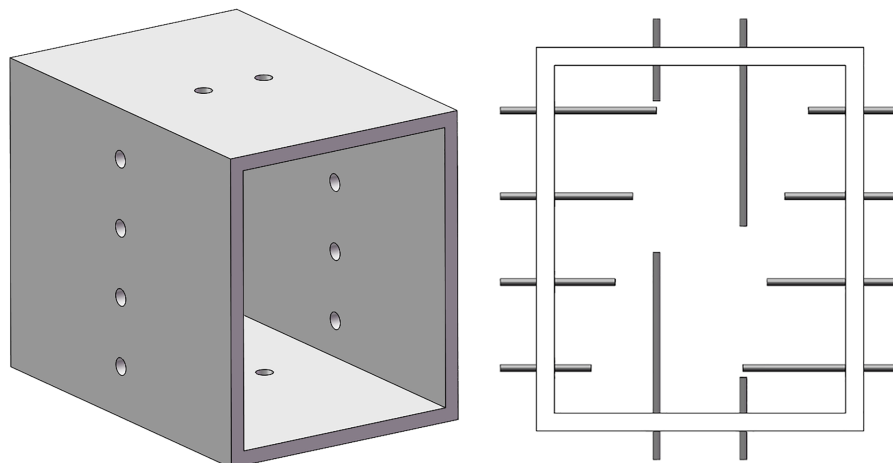


FIG. 4: Temperature measurement points

iteration of the aforementioned measurement and recording steps is repeated until the experiment for all operating conditions is completed. Throughout the experiment, continual adjustments to the infrared camera are made to ensure proper focus. During the experimental process, a stable experimental duration of over 20 s was maintained at each recorded point, and experiments under the same conditions were conducted twice within a span of several days. In the data-processing phase, the data obtained from multiple experiments under the same conditions were averaged to mitigate the impact of random errors. This approach ensures a more reliable representation of the experimental conditions and enhances the accuracy of the results.

2.3 Fundamental Equations

The heat transfer in the experiment is equal to the electrical power at both ends of the tube bundle or the enthalpy difference between the air inlet and outlet; considering the small amount of heat loss during the experiment, the heat transfer is defined as

$$Q = \frac{UI + m\Delta H}{2} \quad (1)$$

and the flow rate of air flowing through the test section is defined as follows:

$$V = \frac{m}{\rho A} \quad (2)$$

$$A = A_t - 6dl \quad (3)$$

where A_t is the cross-sectional area of the test section, d and l are the diameter and length of the tube bundle, respectively. When there are n tubes in the test section, the total heat transfer area is

$$S = n\pi dl \quad (4)$$

and the convection heat-transfer coefficient outside the tube of the air transverse tube bundle is

$$h = \frac{Q}{S(T_w - T_f)} \quad (5)$$

where T_w is the wall temperature and T_f is the qualitative temperature of air. Nusselt number is adopted to represent the heat-transfer characteristics and it is defined as

$$Nu = \frac{hd}{\lambda} = cRe^r \quad (6)$$

$$Re = \frac{\rho V d}{\mu} \quad (7)$$

Finally, the dimensionless Euler (Fei et al., 2014) number calculated from the pressure difference between the inlet and outlet of the test section is used to characterize the flow characteristics:

$$Eu = \frac{\Delta P}{\frac{1}{2} z \rho V^2} \quad (7)$$

where z represents the tube row number in the flow direction.

2.4 Uncertainty Calculation

Uncertainty analysis was conducted to estimate the uncertainties in the experimental results, following the approach from a previous study (Bich et al., 2012):

$$\sigma_y = \sqrt{\sum_{i=1}^N \left(\frac{\delta f}{\delta x_i} \right)^2 \sigma_{xi}^2} \quad (8)$$

$$y = f(x_1, x_2, x_3, \dots, x_n) \quad (9)$$

where x_i represents the measurement variables. In this study, the independent variables consist of temperature, pressure, pressure difference, and mass-flow rate, while the dependent variables include the averaged heat-transfer rate, heat-transfer coefficient, Nusselt number, and Euler number. Under uniform pressure and temperature in all experimental conditions of this study, the physical property parameters of air were obtained from experimental data provided by the National Institute of Standards and Technology (NIST) (Lemmon and Jacobsen, 2004; Lemmon et al., 2007), with a maximum relative difference of no more than 2%.

Results of the accuracy of the infrared camera and thermocouple used in the calibration experiment are shown in Fig. 5. The uncertainty data for the measurement equipment used in the experiment are listed in Table 2. For the measurement instruments used to assess pressure, flow rate, and temperature, we have considered the manufacturer-provided specifications and the results from repeatability experiments. Based on these assessments, we establish that the confidence interval for the measurement accuracy ranges displayed in the table is 95%.

By combining the uncertainty data of the equipment in the experimental system from Table 2, the maximum relative uncertainties of the heat-transfer rate, heat-transfer coefficient, Nusselt number, and Euler number are 0.10, 1.42, 2.65, and 5.74% across all experimental conditions, respectively.

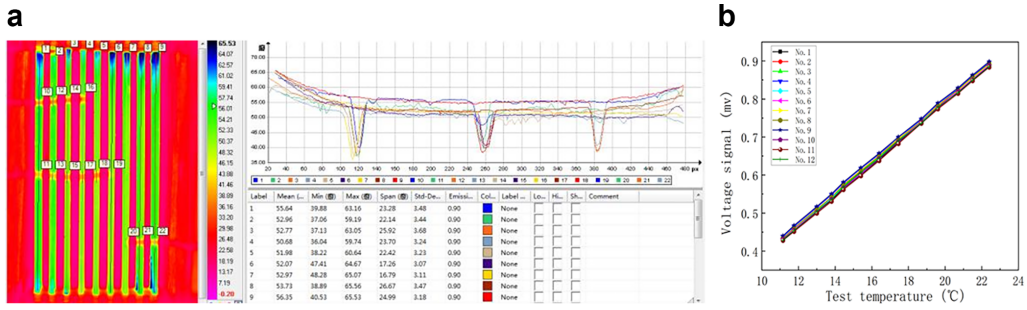


FIG. 5: Temperature-measuring equipment working picture and test calibration results: (a) infrared thermal imager calibration experiment, and (b) thermocouple calibration experiment

TABLE 2: Uncertainties and ranges of air-side direct measurements

Measuring instrument	Direct measurement	Uncertainty
Flowmeter	Mass-flow rate	$\pm 1.5\%$
T-type sheathed thermocouple	Temperature	$\pm 1.5\text{K}$
Infrared thermal imager	Wall temperature	$\pm 0.5\%$
Rosemount 3051CA4 pressure transmitter	Absolute pressure	$\pm 0.25\%$
Rosemount 3051CD4 pressure transmitter	Pressure drop	$\pm 0.075\%$
Multimeter	Voltage	0.001 V
Vernier caliper	Length	0.02 mm

3. RESULTS AND DISCUSSION

This study mainly focuses on the diameter size and arrangement of the tube bundle with a staggered configuration, investigating the flow and heat-transfer variations caused by different tube diameters, transverse distance, and longitudinal row numbers. The experimental parameters are listed in Table 3. In order to minimize random errors, the average value of the data recorded in the first 20 s of each experiment is taken as the final result. Additionally, the average value obtained from multiple shots using the infrared thermal imager is also selected as the final result. The experimental results are presented and analyzed in the following sections of this paper.

TABLE 3: Parameters varied in all experiments

Serial number	Tube diameter (mm)	Transverse distance	Row numbers	Mass-flow rate of air (kg/s)
1	2	$S_1/d = 3$	12	0.06–0.18
2	3	$S_1/d = 3$	12	0.06–0.18
3	5	$S_1/d = 2$	12	0.06–0.18
4	5	$S_1/d = 3$	4, 6, 8, 10, 12	0.06–0.18

3.1 Different Tube Diameters

The experimental results for tube diameters of 2, 3, and 5 mm were integrated as shown in Fig. 6, which presents the heat-transfer characteristics of the test section under different air-flow rates and tube diameters. Figure 6(a) depicts the variation trend of the tube-bundle wall temperature. For the forked tube bundles with the same diameter, the average wall temperature notably decreased with an increase in the incoming flow rate. This result is consistent with the findings of Žukauskas (1987), indicating that the convective heat-transfer coefficient and flow rate exhibit an exponential relationship. As the flow rate increases, the cooling capacity of the air on the tube bundle also increases, resulting in a decrease in the wall temperature. However, as the temperature rise of the air is influenced by both heat transfer and flow conditions, an overall decreasing trend in temperature rise is observed with increasing flow rate as shown in Fig. 6(b). Figure 6(c) vividly illustrates the significant enhancement of the convective heat-transfer coefficient with higher mass-flow rates. This can be attributed to the increased turbulence in the air, resulting in a thinner boundary layer and intensified heat transfer outside the tube. These findings are further supported by Fig. 6(d), which depicts a positive correlation between Nu and Re of air, exhibiting an approximate exponential relationship.

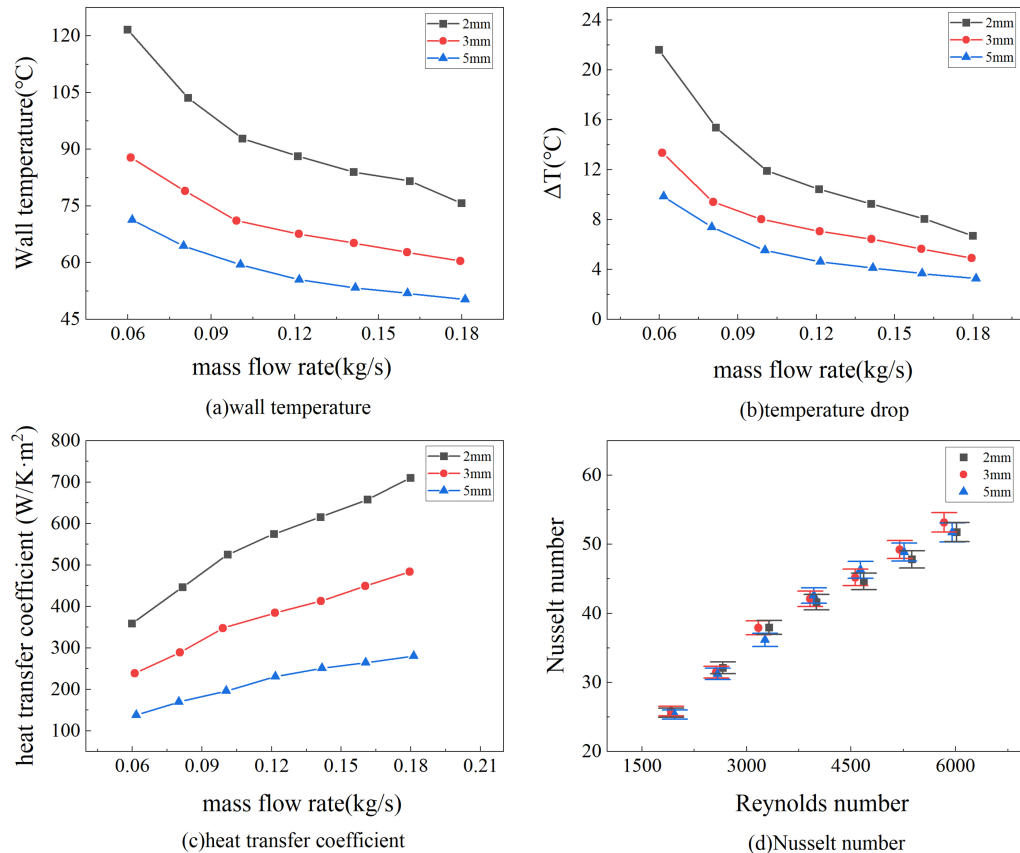


FIG. 6: Heat-transfer characteristics of different tube diameters: (a) wall temperature, (b) temperature drop, (c) heat-transfer coefficient, and (d) Nusselt number

As shown in Fig. 6(c), it can be observed that the smaller the diameter of the tube bundle, the larger the average convective heat-transfer coefficient outside the tube. This conclusion is derived from the relationship between Nusselt number and characteristic size. However, we noted that the relative ratio of convective heat-transfer coefficient between different tube diameters does not correspond to the ratio of tube diameters. This is also caused by increased turbulence as the air velocity increases. In other words, reducing the diameter of the heat-exchange tube directly increases the convective heat-transfer coefficient outside the tube, thereby strengthening the overall heat-transfer capacity of the tube bundle.

Figure 6(d) presents the Nusselt number outside the tube for different diameters. Within the range of diameter variation considered in the test, there is no significant difference in the dimensionless number indicating the heat-transfer characteristics outside the tube. However, the test results for tube diameters below 5 mm exhibit noticeable deviation when compared with the traditional empirical formula proposed by Žukauskas (1987).

Figure 7 presents the impact of various tube diameters on pressure drop. It is commonly accepted that the external flow resistance of the bundle comprises two distinct components: friction resistance and differential pressure resistance. Frictional resistance arises from the viscosity-induced frictional force between the fluid and the surfaces of the tubes. Differential pressure resistance results from the continuous contraction and expansion of the flow-channel area as the fluid passes through the tube bundle, leading to fluctuations in kinetic energy and pressure potential energy.

When the tube diameter remains constant, the pressure drop exhibits an exponential increase with the rise in mass-flow rate, in line with previous research findings that indicate flow resistance is proportional to the square of the velocity. However, as the tube diameter increases from 2 to 5 mm, the pressure loss notably decreases. This suggests that, under certain flow conditions, the change in cross-sectional area of the flow passage results in a reduction in the proportion of fluid in the main flow area, leading to higher friction resistance. Simultaneously, the narrowing of the flow passage elevates the pressure difference resistance of the air in the flow gap of the tube bundle, resulting in an overall increase in total pressure drop.

A further investigation into the variation pattern of the dimensionless Euler number is shown as Fig. 7(b), which characterizes the flow behavior outside the tube. The Euler number initially increases and then stabilizes as the Reynolds number increases, with a more pronounced effect in larger tube diameters. However, when the Reynolds number exceeds 3300, the Euler number shows little variation, and the difference between the Euler numbers of different tube diameters becomes negligible. This suggests that the momentum loss rate does not increase infinitely with

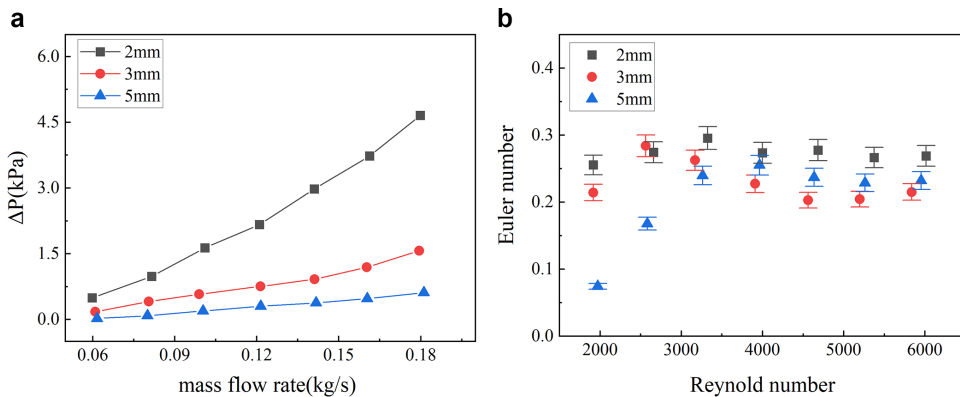


FIG. 7: Flow characteristics of different tube diameters: (a) pressure drop, and (b) Euler number

changes in Reynolds number or flow area as the fluid passes through the tube bundle, but instead has an upper limit. Further analysis is required to elucidate the underlying mechanisms governing this behavior.

3.2 Different Transverse Distance S_1

In order to explore the influence of S_1 on the flow heat transfer of cross-tube bundle, the transverse spacing of tube with 5 mm diameter was reduced to $S_1/d = 2$. Figure 8 shows the flow and heat-transfer characteristics of air passing across the bundle at two different intervals. Figure 8(a) and 8(b) summarize the heat-transfer characteristics of the air under different S_1 . Obviously, the reduction of the space does not change the convective heat-transfer coefficient of the air, while the Nusselt number decreases slightly with the reduction of the space.

Figure 8(c) and 8(d) show the changing law of flow characteristics outside the tube. Obviously, the narrowing of space will lead to a significant increase in air-pressure loss and Euler number, which is consistent with the traditional theory: the resistance and pressure resistance are positively correlated with the flow rate of air; that is, the greater the flow rate, the greater the total flow resistance. The law of change of Euler number is the same as in the previous section, that is,

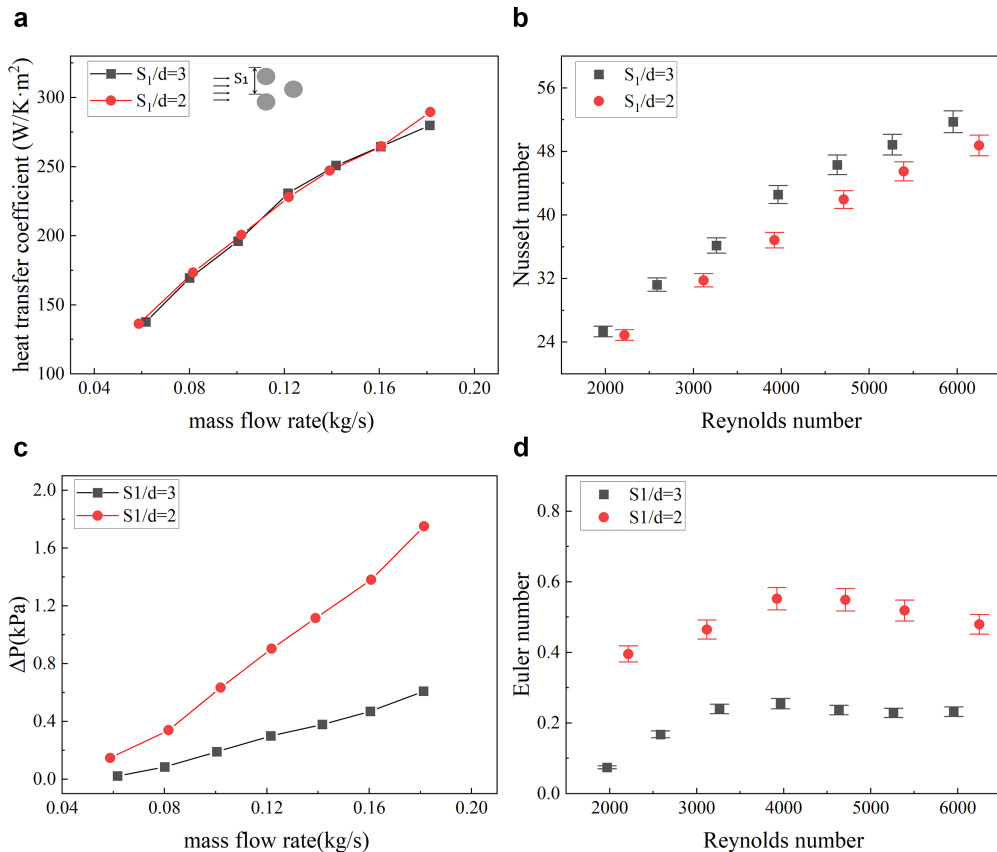


FIG. 8: Experimental data of flow heat-transfer characteristics under different working conditions of S_1 : (a) Heat-transfer coefficient, (b) Nusselt number, (c) pressure drop, and (d) Euler number

it does not always increase with the increase of Reynolds number, but gradually becomes stable. And, the corresponding variation trend of different horizontal spacing is very close.

According to the conclusions of some computational fluid dynamics (CFD) studies (Bacellar et al., 2016), it can be known that the fast velocity distribution and violent turbulent pulsation under large flow rate will make the mass and heat transfer between the impact zone at the front end of the bundle, the wake zone at the back end of the bundle, and the main-stream zone with high efficiency.

3.3 Different Numbers of Row

In Žukauskas (1987), a correction factor μ was introduced into the Nusselt number formula for tube rows with fewer than 20 rows to eliminate the influence caused by the excessively low heat-transfer intensity of the first row of tubes. The number of tube rows is also taken as one of the key points in this experiment with 5 mm tubes. The flow heat-transfer characteristics of 4, 6, 8, and 10 rows of tube rows were studied, respectively, in order to explore the influence of the number of tube rows on the test results, and compared with the correction factor proposed by Žukauskas (1987).

In Fig. 9(a), the convective heat-transfer coefficient is shown to change with the air-flow rate under different tube rows. When the tube rows increase, the convective heat-transfer coefficient also increases significantly under the same flow rate. And, the difference becomes negligible when the tube rows exceed 10, indicating that increasing the number of tube rows has a significant strengthening effect on heat transfer, especially when the number of tube rows is small. Figure 9(b) shows the variation rule of Nusselt number, which is as same as the convective heat-transfer coefficient. Figure 9(b) depicts the variation of the Nusselt number, which follows the same trend as that of the convective heat-transfer coefficient. The research of Žukauskas (1987) revealed that the correction coefficient of rows is 0.98 when the number of rows exceeds 10, whereas it is 0.89 when the number of rows is 4; this finding agrees with the data of our investigation.

Figure 10 illustrates the effect of tube row number on flow resistance. Figure 10(a) shows the variation of pressure drop with air flow under different tube rows. It is evident that the pressure drop increases significantly with the increase in the number of tube rows under the same flow velocity. This phenomenon can be attributed to the increase in friction resistance and instability of the flow field caused by the increased number of tube rows. Moreover, the effect of varying

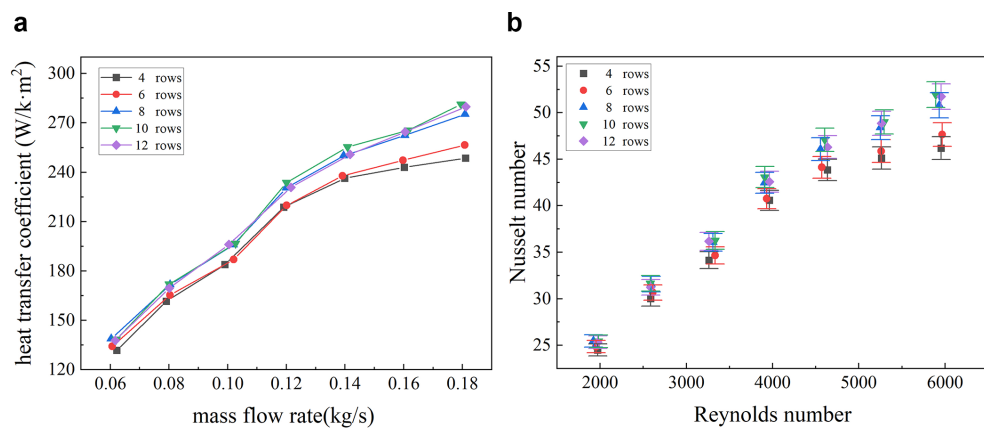


FIG. 9: Experimental data of heat-transfer characteristics under different working conditions of rows: (a) heat transfer coefficient, and (b) Nusselt number

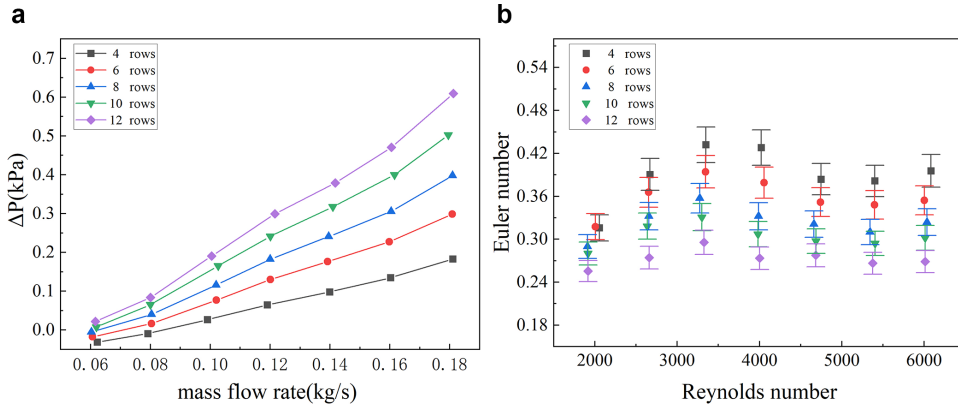


FIG. 10: Flow characteristics of different numbers of row: (a) pressure drop, and (b) Euler number

row numbers on pressure drop also depends on the air flow rate. Specifically, the difference in pressure drop between different row numbers is more prominent at higher air-flow rates.

The plot of dimensionless Euler number versus Reynolds number for different tube arrangements is shown in Fig. 10(b). The trend of the Euler number is similar to the previous finding. When Re is less than 3500, it rises rapidly, then decreases slightly, and finally stabilizes. The Euler number is significantly influenced by the number of tube rows, and fewer tube rows result in larger Euler numbers and greater fluctuations in Euler number changes. These findings demonstrate that, in the fork row system, increasing the number of longitudinal tube rows can stabilize the flow resistance with changes in air velocity.

3.4 Proposed New Correlation

In Fig. 11(a)–11(c), the external heat-transfer coefficient Nu under different tube diameters mentioned in Sec. 3.1 are compared with four existing formulas obtained by Žukauskas (1987), Bacellar et al. (2016), Khan et al. (2006), and Wung and Chen (1989) in their respective studies. The exact form of these existing formulas in the range of Reynolds numbers covered in this study is as follows. Due to the complex form of Bacellar's formula, the constants in the formula are not listed in detail in this article.

Žukauskas:

$$Nu = 0.35 \left(\frac{S_1}{S_2} \right)^{0.2} Re_f^{0.6} Pr_f^{0.36} \left(\frac{Pr_f}{Pr_w} \right)^{0.25} \quad (10)$$

Bacellar:

$$Nu = C_1 Re_{D,c}^{P_1} N^{P_2} \left(\frac{P_l}{D} \right)^{P_3} \left(\frac{P_l}{D} \right)^{P_4} \left(\frac{P_l}{P_t} \right)^{C_2} \quad (11)$$

Khan:

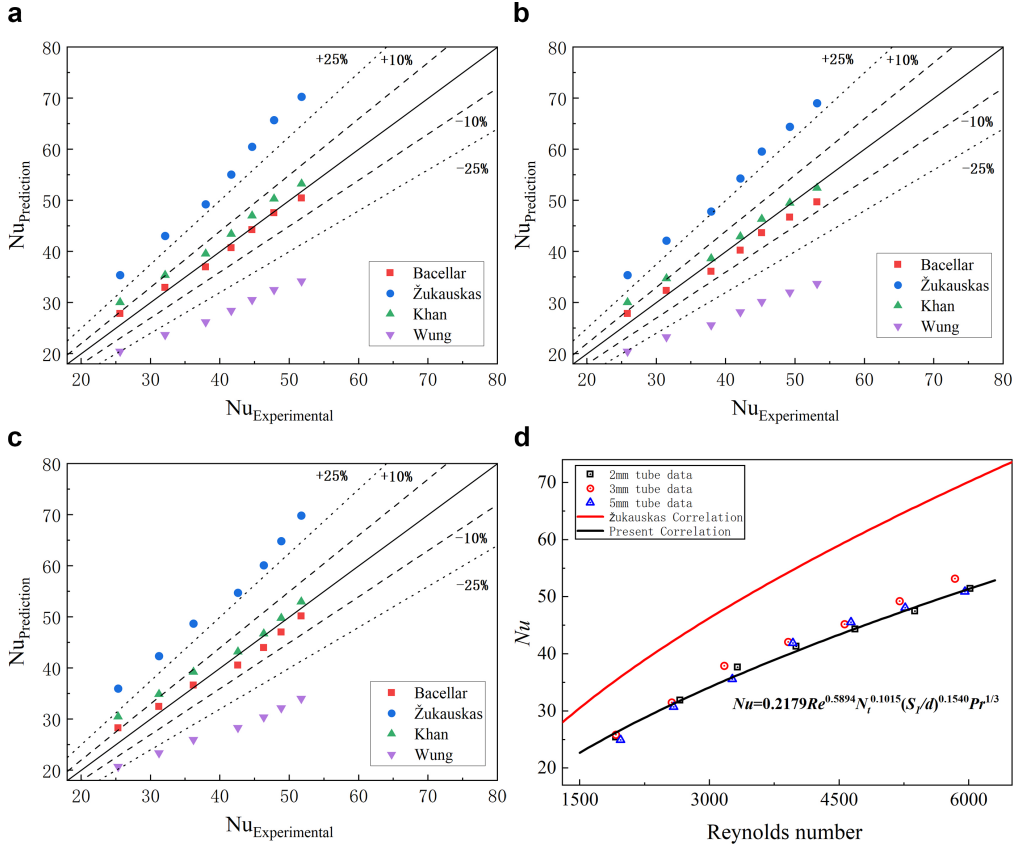


FIG. 11: Proposed new correlations for small-diameter tube. (a) Deviation from existing formulas of 2 mm, (b) deviation from existing formulas of 3 mm, (c) deviation from existing formulas of 5 mm, and (d) new correlations for Nusselt number

$$Nu = 0.61 \frac{\left(\frac{S_l}{D}\right)^{0.144}}{1 - 2 \cdot \exp\left(-1.09 \cdot \frac{S_l}{D}\right)} Re_D^{1/2} Pr^{1/3} \quad (12)$$

Wung:

$$Nu = 0.78 Re_D^{0.45} Pr^{1/3} \quad (13)$$

Within the scope of this work, the formulas by Bacellar and Khan exhibit good accuracy in predicting heat transfer outside the tubes, also indicating the availability of experimental data. Notably, Bacellar's prediction method shows a deviation of less than 3% for the micro-tube bundle compared with the present correlation, despite its highly intricate formula. A simpler correlation based on experimental data is of greater application value.

In order to directly and accurately reflect the influence of various variables in the staggered tube-bundle system on the heat transfer outside the tube, we fit a new Nusselt number correlation for small-tube diameter based on the following form:

$$Nu = \alpha Re^\beta N_t^\gamma (S_t/d)^\delta Pr^{1/3} \quad (14)$$

where N_t represents the numbers of tube banks and Pr represents the Prandtl number.

According to the experimental results in this study, the external Nusselt number correlation suitable for small-tube diameters is proposed, which has a high predictive accuracy for the current data.

$$Nu = 0.2179 Re^{0.5894} N_t^{0.1015} (S_t/d)^{0.1540} Pr^{1/3} \quad (15)$$

In Fig. 11(d), the heat-transfer data obtained from this experiment are fitted, and the new relationship describing the exponential correlation between the Nusselt number and the Reynolds number is compared with the traditional formula. It is evident that the external heat-transfer empirical curve for all small-tube diameters deviates from the empirical curve for external convection heat transfer of the fork bank summarized by the traditional Žukauskas. The diameter deviation for a 2 mm tube is -14%, the diameter deviation for a 3 mm tube is -11%, and the diameter deviation for a 5 mm tube is -10%. As the diameter of the tube decreases, the applicability of the traditional formula deteriorates.

For demonstrating the accuracy of the correction coefficients for S_t and N_t suggested in the correlation, Fig. 12 was utilized with $Nu/(S_t/d)^{0.1540}$ and $Nu/N_t^{0.1015}$ plotted as the respective ordinates. Additionally, a comparison was made between the fitting formula and some of the data presented above. It is evident that the new correlation exhibited a robust linear relationship with a maximum error of no more than 5%, thereby demonstrating reliable prediction accuracy. It can be observed that although previous studies have introduced a broader range of variables, they of-

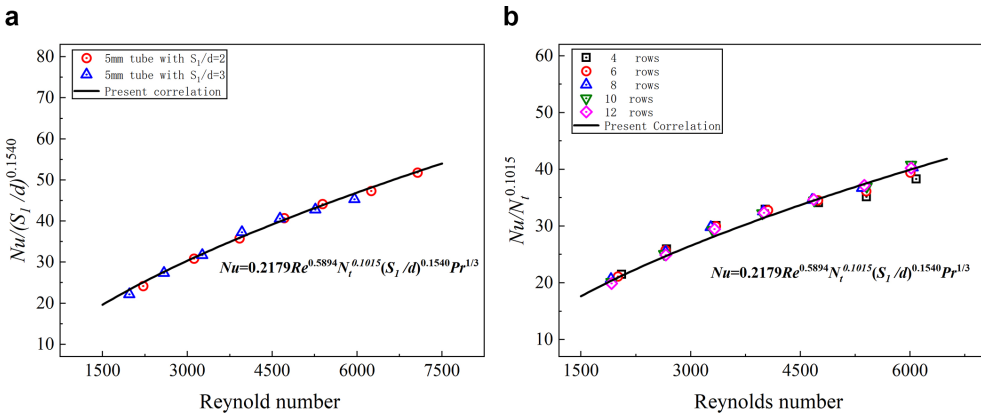


FIG. 12: Accuracy verification of the present correlation: (a) new correlations for different S_t/d , and (b) new correlations for different N_t

ten lacked considerations for corrections related to the number of tube rows and tube diameters. Additionally, inherent discrepancies between numerical simulations and experimental research inevitably exist. This can lead to variations in the results, especially when applying these models to real-world scenarios, necessitating a more nuanced approach in both theoretical and practical applications of heat-transfer models in small-diameter tube bundles. Practically, these findings are particularly relevant for the design of compact heat exchangers, like those commonly used in modern aircraft. The correlation provides robust support in the design process, ensuring efficient and reliable performance in these critical applications, where precise heat-transfer control is paramount. This aligns well with the ongoing trend towards miniaturization and efficiency in thermal management systems.

To summarize, while maintaining a high level of consistency with previous numerical investigations, the findings of this study contribute significant engineering insights for research in the small-diameter range. These results hold great practical value and provide a strong theoretical foundation for the study of compact heat exchangers.

4. CONCLUSION

In light of the advancements in compact heat-exchanger technologies, it has become increasingly vital to specifically explore the heat-transfer characteristics of small-diameter tube bundles for more accurate and relevant findings. In this work, experimental investigations were conducted to analyze the air-side heat transfer and pressure-drop characteristics of small-diameter tube bundles arranged in a staggered configuration and exposed to cross flow. The independent variables considered in the experiments were the air-flow rate, Reynolds number, tube diameter, transverse spacing, and longitudinal row number. A Nusselt number fitting formula, suitable for the tubular diameter, was derived, and the comprehensive performance was compared and analyzed. Based on the experimental data, the following conclusions were drawn:

1. As the fluid flows through the tube bundle, the heat-transfer efficiency on the outer surface of the tubes increases with an increase in the flow rate. Additionally, smaller tube diameters lead to higher convective heat-transfer coefficients. When the tube diameter remains the same, the influence of transverse spacing S_1 on heat transfer is not significant. Furthermore, the convective heat-transfer coefficient increases with the number of rows when it is between 4 and 12.
2. The Nusselt number calculation results in all the test data have shown a certain deviation from the traditional Žukauskas formula, ranging from -14 to -10% . The Nusselt number calculation results in all the test data have shown a certain deviation from the traditional Žukauskas formula, ranging from -14 to -10% . Moreover, the deviation in the prediction of the traditional formula is greater for smaller tube diameters. The correlation proposed by this study for microtube bundle is in good agreement with the experimental data and some numerical studies.
3. The pressure drop outside the tube increases exponentially with air-flow rate and is also influenced by the tube diameter, transverse spacing, and number of tube rows. The Euler number difference under different test conditions is similar to the pressure-drop difference, except that the Euler number always increases first and then becomes stable as flow velocity increases.
4. Our study extends to guiding heat-exchanger design, particularly in thermal calculations. Designers and engineers can utilize the newly developed formulas to verify and refine their designs, ensuring optimized performance and efficiency. This approach is especially beneficial for compact heat-exchanger systems, where precise heat-transfer calculations are critical for maximizing performance within constrained spatial dimensions.

ACKNOWLEDGMENTS

The authors appreciate the supports from the National Science and Technology Major Project of China (Nos. 2017-III-0005-0029, J2019-III-0021-0065, and J2019-III-0015-0059), the Fundamental Research Funds for the Central Universities, and the Science Center for Gas Turbine Project (No. P2022-C-II-005-001).

REFERENCES

- Bacellar, D., Aute, V., Huang, Z., and Radermacher, R., Airside Friction and Heat Transfer Characteristics for Staggered Tube Bundle in Crossflow Configuration with Diameters from 0.5 mm to 2.0 mm, *Int. J. Heat Mass Transf.*, vol. **98**, pp. 448–454, 2016.
- Bacellar, D., Aute, V., and Radermacher, R., CFD-Based Correlation Development for Air Side Performance of Finned and Finless Tube Heat Exchangers with Small Diameter Tubes, in *15th Int. Refrigeration and Air Conditioning Conf.*, West Lafayette, IN: Purdue University, p. 2240, 2014.
- Bich, W., Cox, M.G., Dybkaer, R., Elster, C., Estler, W.T., Hibbert, B., Imai, H., Kool, W., Michotte, C., and Nielsen, L., Revision of the ‘Guide to the Expression of Uncertainty in Measurement’, *Metrologia*, vol. **49**, p. 702, 2012.
- Bruening, G.B. and Chang, W.S., Cooled Cooling Air Systems for Turbine Thermal Management, *Proc. of the ASME 1999 Int. Gas Turbine and Aeroengine Congress and Exhibition*, vol. **78606**, p. V003T01A002, 1999.
- Chang, N.-C., Li, C.-J., and Wang, C.-C., Performance of Bare-Tube Bundle Having Small Diameter Tube: With and Without Partial Bypass, *Int. Commun. Heat Mass Transf.*, vol. **67**, pp. 73–80, 2015.
- Chen, C.J. and Wung, T.-S., Finite Analytic Solution of Convective Heat Transfer for Tube Arrays in Crossflow: PartII—Heat Transfer Analysis, *J. Heat Transf.*, vol. **111**, no. 3, pp. 641–648, 1989.
- Chen, Y., Fiebig, M., and Mitra, N., Heat Transfer Enhancement of Finned Oval Tubes with Staggered Punched Longitudinal Vortex Generators, *Int. J. Heat Mass Transf.*, vol. **43**, pp. 417–435, 2000.
- Da-Peng, L., Zeng-Geng, J., and Feng-Rui, S., Investigations on Heat Transfer and Fluid Flow over Banks of Staggered Tubes Using the Finite Element Method, *Energy Res. Inform.*, vol. **19**, pp. 53–56, 2003.
- Deeb, R., Numerical Analysis of the Effect of Longitudinal and Transverse Pitch Ratio on the Flow and Heat Transfer of Staggered Drop-Shaped Tubes Bundle, *Int. J. Heat Mass Transf.*, vol. **183**, p. 122123, 2022.
- Fei, L., Fengzhong, S., and Yuetao, S., Experimental Research and Synergy Analysis on Characteristics of Tube Bundles, *J. Shandong Univ. (Eng. Sci.)*, vol. **44**, pp. 70–75, 2014.
- Fu, Y., Liu, W., Qi, H., Chen, Q., Wen, J., and Xu, G., Heat Transfer Area Optimization of Intermediate Heat-Exchange Cycle System for Aero Engines, *Int. J. Heat Mass Transf.*, vol. **220**, p. 124995, 2024.
- Grimison, E., Correlation and Utilization of New Data on Flow Resistance and Heat Transfer for Cross Flow of Gases over Tube Banks, *Trans. American Soc. Mech. Eng.*, vol. **59**, pp. 583–594, 1937.
- Ishak, M., Tahseen, T.A., and Rahman, P.D.M.M., Experimental Investigation on Heat Transfer and Pressure Drop Characteristics of Air Flow over a Staggered Flat Tube Bank in Crossflow, *Int. J. Automot. Mech. Eng.*, vol. **7**, pp. 900–911, 2013.
- Khan, M.S., Zou, R., and Yu, A., Computational Simulation of Air-Side Heat Transfer and Pressure Drop Performance in Staggered Mannered Twisted Oval Tube Bundle Operating in Crossflow, *Int. J. Therm. Sci.*, vol. **161**, p. 106748, 2021.
- Khan, W.A., Culham, J.R., and Yovanovich, M.M., Convection Heat Transfer from Tube Banks in Crossflow: Analytical Approach, *Int. J. Heat Mass Transf.*, vol. **49**, pp. 4831–4838, 2006.
- Lai, J., Sun, L., Gao, L., and Li, P., Mechanism Analysis on Fluidelastic Instability of Tube Bundles in Considering of Cross-Flow Effects, *Nucl. Eng. Technol.*, vol. **51**, pp. 310–316, 2019.
- Lemmon, E., Huber, M.L., and McLinden, M.O., NIST Standard Reference Database 23: Reference Fluid Thermodynamic and Transport Properties-REFPROP, version 8.0, 2007.

- Lemmon, E.W. and Jacobsen, R.T., Viscosity and Thermal Conductivity Equations for Nitrogen, Oxygen, Argon, and Air, *Int. J. Thermophys.*, vol. **25**, pp. 21–69, 2004.
- Li, H., Huang, H., Xu, G., Wen, J., and Wu, H., Performance Analysis of a Novel Compact Air-Air Heat Exchanger for Aircraft Gas Turbine Engine Using LMTD Method, *Appl. Therm. Eng.*, vol. **116**, pp. 445–455, 2017.
- Li, N., Zhao, Y., Wang, H., Chen, Q., Li, Z., Ma, Y., and Tang, G., Thermal and Hydraulic Performance of a Compact Precooler with Mini-Tube Bundles for Aero-Engine, *Appl. Therm. Eng.*, vol. **200**, p. 117656, 2022.
- Liu, W., Xu, G., Fu, Y., Wen, J., and Zhang, N., Numerical Investigation on Forced, Natural, and Mixed Convective Heat Transfer of N-Decane in Laminar Flow at Supercritical Pressures, *Int. J. Heat Mass Transf.*, vol. **209**, p. 124129, 2023.
- Liu, Y., Fu, Y., Huang, H., Wen, J., and Xu, G., A Novel Air-Air Heat Exchanger Design and Experimental Validation for Aero-Engines, in *ASME Intl. Mechanical Engineering Congress and Exposition, American Society of Mechanical Engineers*, no. V08AT10A040, 2018.
- Liu, Y., Xu, G., Fu, Y., Wen, J., Qi, S., and Lyu, L., Airside Pressure Drop Characteristics of Three Analogous Serpentine Tube Heat Exchangers Considering Heat Transfer for Aero-Engine Cooling, *Chin. J. Aeronaut.*, vol. **35**, pp. 32–46, 2022.
- Pan, W., Chi, Z.-H., and Si, D.-B., Numerical Simulation of Uneven Entry Velocity Distribution Gas Flowing Across Different Arrayed Tube Bundles, *J. Zhejiang Univ. Eng. Sci.*, vol. **38**, pp. 1043–1046, 2004.
- Qing, X., Changming, L., and Dongmei, Z., Heat Transfer and Pressure Drop in Trapezoidal Duct with Pin-Fin Arrays Along the Flow, *Energy Metall. Ind.*, vol. **26**, pp. 21–25, 2007.
- Qiwi, D. and Yangke, O., Numerical Investigation of Fluid Flow Across Tube Bundles in Zukauskas Experimental Model, *Press. Vessel Technol.*, vol. **27**, pp. 21–26, 2010.
- Saraireh, M.A., Alsaraireh, F.M., and Alrwashdeh, S.S., Investigation of Heat Transfer for Staggered and In-Line Tubes, *Int. J. Mech. Eng. Technol.*, vol. **8**, pp. 476–483, 2017.
- Wen, J., Huang, H., Li, H., Xu, G., and Fu, Y., Thermal and Hydraulic Performance of a Compact Plate Finned Tube Air-Fuel Heat Exchanger for Aero-Engine, *Appl. Therm. Eng.*, vol. **126**, pp. 920–928, 2017.
- Wilson, A.S. and Bassiouny, M.K., Modeling of Heat Transfer for Flow Across Tube Banks, *Chem. Eng. Process.: Process Intensif.*, vol. **39**, pp. 1–14, 2000.
- Wu, Z., You, S., Zhang, H., and Zheng, W., Experimental Investigation on Heat Transfer Characteristics of Staggered Tube Bundle Heat Exchanger Immersed in Oscillating Flow, *Int. J. Heat Mass Transf.*, vol. **148**, p. 119125, 2020.
- Wung, T.-S. and Chen, C.J., Finite Analytic Solution of Convective Heat Transfer for Tube Arrays in Cross-flow: Part I—Heat Transfer Analysis, *J. Heat Transf.*, vol. **111**, no. 3, p. 633–640, 1989.
- Xie, J., Li, S., Yan, H., and Xie, G., Numerical Analysis on Thermal–Hydraulic Performances of Staggered Tube Bundles for An Aero-Engine Compact Precooler, *J. Therm. Anal. Calorim.*, vol. **141**, pp. 387–399, 2020.
- Xu, X., En-Lu, W., and Cong, W., The Influences of the Diameter Size on the Convective and Condensation Heat Transfer Characteristic for The Staggered Tube Bundle Heat Exchanger, *Boiler Technol.*, vol. **47**, pp. 1–4, 2016.
- Yangjia, Q., Laihe, Z., Qihang, L., Zhiwei, L., and Jie, W., Numerical Investigation on Heat Transfer Characteristics of Staggered Tube Bundles in Cross Flow, *J. Aerosp. Power*, vol. **38**, pp. 2718–2728, 2023.
- Zeenshan, M., Nath, S., and Bhanja, D., Numerical Analysis to Predict the Optimum Configuration of Fin and Tube Heat Exchanger with Rectangular Vortex Generators for Enhanced Thermohydraulic Performance, *Heat Mass Transf.*, vol. **56**, pp. 2159–2169, 2020.
- Zhang, L., Balachandar, S., Tafti, D., and Najjar, F., Heat Transfer Enhancement Mechanisms in Inline and Staggered Parallel-Plate Fin Heat Exchangers, *Int. J. Heat Mass Transf.*, vol. **40**, pp. 2307–2325, 1997.
- Zhao, C.-Y., Yao, Z.-L., Qi, D., Ji, W.-T., Li, A.-G., and Tao, W.-Q., Numerical Investigation of Tube Bundle Arrangement Effect on Falling Film Fluid Flow and Heat Transfer, *Appl. Therm. Eng.*, vol. **201**, p. 117828, 2022.
- Žukauskas, A., Heat Transfer from Tubes in Crossflow, in *Advances in Heat Transfer*, J.P. Hartnett and T.F. Irvine, Eds., Elsevier, 1987.